Original Article

MOLECULAR METABOLISM

BMP4 gene therapy enhances insulin sensitivity but not adipose tissue browning in obese mice

Jenny M. Hoffmann [1], John R. Grünberg [1], Ann Hammarstedt [1], Tobias Kroon [2], Thomas U. Greiner [3], Stefanie Maurer [2], Ivet Elias [4,5], Vilborg Palsdottir [6], Fatima Bosch [4,5], Jeremie Boucher [1,2,7], Shahram Hedjazifar [1], Ulf Smith [1,*]

ABSTRACT

Objective: Bone morphogenetic protein 4 (BMP4) adeno-associated viral vectors of serotype 8 (AAV8) gene therapy targeting the liver prevents the development of obesity in initially lean mice by browning the large subcutaneous white adipose tissue (WAT) and enhancing energy expenditure. Here, we examine whether this approach could also reduce established obesity.
Methods: Dietary-induced obese C57BL6/N mice received AAV8 BMP4 gene therapy at 17–18 weeks of age. They were kept on a high-fat diet and phenotypically characterized for an additional 10–12 weeks. Following termination, the mice underwent additional characterization in vitro.
Results: Surprisingly, we observed no effect on body weight, browning of WAT, or energy expenditure in these obese mice, but whole-body insulin sensitivity and glucose tolerance were robustly improved. Insulin signaling and insulin-stimulated glucose uptake were increased in both adipose cells and skeletal muscle. BMP4 also decreased hepatic glucose production and reduced gluconeogenic enzymes in the liver, but not in the kidney, in addition to enhancing insulin action in the liver.
Conclusions: Our findings show that BMP4 prevents, but does not reverse, established obesity in adult mice, while it improves insulin sensitivity independent of weight reduction. The BMP antagonist Noggin was increased in WAT in obesity, which may account for the lack of browning.

Keywords Obesity; Gene therapy; Insulin sensitivity; Adipose tissue; Skeletal muscle; Liver

1. INTRODUCTION

White adipose tissue (WAT) expansion can occur through enlargement of existing adipocytes (hypertrophic expansion) and/or by recruitment and differentiation of new adipocytes (hyperplastic expansion) [1]. White adipocytes have a mesenchymal stem cell origin [2], and the complex molecular events regulating commitment and differentiation are still unclear. One of the early, and central, events in white adipocyte commitment is the action of bone morphogenetic protein 4 (BMP4), which results in the activation of peroxisome proliferator–activated receptor gamma (PPARg) and commitment of preadipocytes [2,3]. Interestingly, BMP4 is secreted by mature adipocytes and increased in hypertrophic obesity [4], thereby eliciting a positive feedback signal to recruit new adipocytes. We have also previously shown that primary human preadipocytes, isolated from the subcutaneous (SubQ) WAT depot, undergo improved differentiation in vitro when treated with BMP4 [5], consistent with data in other models [2]. Hypertrophic adipocytes have increased endogenous BMP4 gene expression and secretion. However, BMP4 signaling is antagonized by increased secretion of BMP antagonists, and two of these antagonists are Noggin [5,6] and Gremlin 1 [7]. We found Gremlin1 to be increased in human hypertrophic WAT [4], whereas in the mouse, WAT Noggin, but not Gremlin1, is increased [8].

We and others have described that BMP4 also has a role in enhancing beige adipogenesis in human preadipocytes [4], transgenic mice overexpressing *Bmp4* in WAT [9], as well as in lean mature mice following BMP4 gene therapy [8]. In the latter study, we treated adult, lean mice with adeno-associated viral vectors of serotype 8 (AAV8) carrying the *Bmp4* gene and targeting the liver, resulting in increased circulating BMP4 levels, which targeted the SubQ WAT and induced browning. The mice had increased energy expenditure and were protected from diet-induced obesity, despite the finding that BMP4 actually inhibits BAT activation, as also shown in direct in vitro experiments [10]. However, these results support a beneficial effect of BMP4 only in preventing obesity. Its potential role in treating obesity and insulin resistance is still unknown.

[1]The Lundberg Laboratory for Diabetes Research, Department of Molecular and Clinical Medicine, the Sahlgrenska Academy, University of Gothenburg, Gothenburg, Sweden [2]Bioscience Metabolism, Research and Early Development, Cardiovascular, Renal and Metabolic (CVRM), BioPharmaceuticals R&D, AstraZeneca, Gothenburg, Sweden [3]The Wallenberg Laboratory, Department of Molecular and Clinical Medicine, The Sahlgrenska Academy, University of Gothenburg, Gothenburg, Sweden [4]Center of Animal Biotechnology and Gene Therapy and Department of Biochemistry and Molecular Biology, School of Veterinary Medicine, Universitat Autònoma de Barcelona, 08193, Bellaterra, Spain [5]Centro de Investigación Biomédica en Red de Diabetes y Enfermedades Metabólicas Asociadas (CIBERDEM), Spain [6]Department of Physiology/Endocrinology, The Sahlgrenska Academy, University of Gothenburg, Gothenburg, Sweden [7]Wallenberg Centre for Molecular and Translational Medicine, University of Gothenburg, Sweden

*Corresponding author. The Lundberg Laboratory for Diabetes Research, Department of Molecular and Clinical Medicine, Sahlgrenska University Hospital, Blå Stråket 5, SE-413 45, Gothenburg, Sweden. E-mail: ulf.smith@medic.gu.se (U. Smith).

Received October 30, 2019 • Revision received November 21, 2019 • Accepted November 22, 2019 • Available online 17 December 2019

https://doi.org/10.1016/j.molmet.2019.11.016

Therefore, in the present study, we tested whether BMP4 gene therapy could also be used to treat already established obesity. Our results show that obesity is not reduced but that BMP4 improves whole-body insulin sensitivity, enhances insulin signaling in all key metabolic tissues, and reduces key gluconeogenic enzymes in the liver despite no weight loss.

2. RESULTS

The mice were fed a high-fat diet (HFD) for 11 weeks prior to the AAV8 injections to allow increased body weight. Body weights and blood glucose levels were used to match the two groups for the AAV8 BMP4 and AAV8 control injections for cohort 1 (at study week 0; Fig. S1a and b) and later also for a second cohort of mice (cohort 2, also injected at study week 0; Fig. S2a and f). Schematic figures of the study designs for cohorts 1 and 2 are shown in Figs. S1c and S2b. Although initial design and matching of the mice were similar, different phenotyping procedures were performed, and cohort 2 was used to examine hepatic glucose production through a pyruvate tolerance test and for labeled tissue glucose uptake.

2.1. Increased hepatic and serum BMP4 levels following AAV8 BMP4 injections, but not in peripheral tissues

Twelve weeks after tail-vein injection of 5×10^{11} vg/mice of AAV8 Ctrl and AAV8 BMP4, vector genome copy number was determined in liver and epididymal fat (Epi) of injected mice from cohort 1. As shown in Figure 1A, we found a very high transduction of the liver (vector genome/diploid genome), while the levels were marginal in Epi WAT. This result is consistent with the high tropism for the liver of the AAV8 vectors after intravascular administration. Moreover, when the expression levels of the mouse codon—optimized BMP4 (moBMP4) were measured by quantitative reverse transcriptase polymerase chain reaction (RT-qPCR) in the liver and Epi WAT of the AAV8 BMP4-treated mice, very high levels were observed in the liver of these mice, while Epi fat again expressed only marginal levels (Figure 1B), which is consistent with the use of the liver-specific human alpha 1-antitrypsin (hAAT) promoter.

Next, we evaluated the effect of the AAV8 BMP4 treatment on serum and tissue protein BMP4 levels in the same mice. As expected, hepatic BMP4 protein (Figure 1C) was markedly increased, but the vectors did not increase BMP4 protein in the other tissues examined, including skeletal muscle (tibialis anterior; TA) or SubQ WAT, similar to previous reports with these vectors [8]. Endogenous BMP4 protein was low in the livers from control animals compared with the AAV8 BMP4 mice (Figure 1C), but it was clearly expressed at the gene level (Ct values around 31 in both groups; see also Figure 3E). This was further verified in an uncut immunoblot of liver BMP4 protein, which clearly showed that it was present as an unprocessed protein in the control animals (Fig. S1d). Endogenous BMP4 was highly expressed in WAT and skeletal muscles (TA), but there was no difference between the groups (Figure 1C). Mice treated with the AAV8 BMP4 vectors had increased circulating BMP4 levels measured at termination as expected (Figure 1D). These results demonstrate that AAV8 BMP4 mice have increased hepatic and circulating BMP4 levels and that the BMP4 expression lasted for the full duration of the study.

2.2. AAV8 BMP4 gene therapy in obese mice does not induce weight loss or browning of WAT

In contrast to our previous findings in which initially lean mice fed a HFD were protected from obesity [8], the current initially obese AAV8 BMP4-treated mice did not reduce their body weights nor were they protected from further weight gain (Figure 1E). Food intake was also not changed compared with the control mice (Figure 1F), nor were there any differences in the weights of Epi or SubQ WAT depots (Figure 1G), in SubQ adipocyte size (Figure 1H), in VO_2 (Figure 1I), or in animal movements (data not shown). Adipocyte size in the Epi depot was not analyzed.

We next examined markers of browning, which were not increased at the transcriptional level in the SubQ WAT (Figure 2A; including UCP1 protein, data not shown), and OXPHOS activation was similar (Figure 2B). We also examined whether BMP4 gene therapy enhanced markers of terminal adipocyte differentiation in the SubQ WAT. As shown in Figure 2C, only the expression of adiponectin and G protein—coupled receptor 120 (*Gpr120*) were significantly increased. There were no differences in markers of WAT fibrosis or inflammation (Figure 2D) nor in circulating levels of SAA3 (Figure 2E). However, AAV8 BMP4 mice had significantly higher serum levels of adiponectin (Figure 2F) and lower levels of free fatty acids (Figure 2G), suggesting enhanced insulin sensitivity.

BMP4 has recently been shown to directly target and inhibit BAT cells [10], which is also seen in lean mice following BMP4 gene therapy [8], leading to increased lipid accumulation and inhibition of its lipolytic and oxidative effects [8,10]. We therefore also examined BAT but saw a similar increase in BAT lipid accumulation in both groups of obese mice (Fig. S1e). Furthermore, both *Ucp1* mRNA (Fig. S1f) and protein (Fig. S1g) were similar, and other mitochondrial and white adipose marker genes, including *Pparg* and *Fabp4*, were also similar (Fig. S1f). Hormone-sensitive lipase (HSL) protein was also not different between the two groups (Fig. S1h). Consistent with findings in WAT, we also saw increased endogenous tissue *Bmp4* and *Noggin* gene expression in BAT in both obese groups compared with lean control mice (Fig. S1i). Thus, BAT in obese mice seems to have already acquired a beige phenotype, which was not further enhanced by AAV8 BMP4, probably because tissue BMP4 is already increased in obesity.

Taken together, these results show that BMP4 gene therapy in initially obese mice does not increase browning of the SubQ WAT or reduce body weight. In addition, BMP4 gene therapy does not reduce fibrosis or inflammation in WAT and also has no impact on markers of BAT function in obesity.

2.3. Reduced BMP signaling in subcutaneous adipose tissue but not in skeletal muscle or in liver

Our current findings suggest the induction of a BMP4 resistance in murine WAT cells in obesity. In fact, similar to BAT, we found increased mRNA levels of endogenous *Bmp4* in WAT in the obese HFD groups compared with a group of lean animals previously studied [5] (CD Ctrl) as well as increased expression of the BMP4 antagonist Noggin (Figure 3A). In line with this, pSMAD1/5/8 levels were reduced in SubQ adipocytes in both obese groups (Figure 3B), and there was no significant difference between the groups. In contrast, neither Noggin nor *BMP4* mRNA levels were different between the groups in skeletal muscle (Figure 3C), and pSMAD1/5/8 was also increased in both groups (Figure 3D).

Endogenous BMP4 mRNA levels were also similar in the liver (Figure 3E), while the expression of Noggin was very low in both lean and obese mice (data not shown) and pSMAD1/5/8 was increased, particularly in the AAV8 BMP4 mice (Figure 3F). Total SMAD protein was unchanged in the liver (Figure 3F).

We also validated that BMP activity in serum from obese untreated HFD mice was lower than that in serum from lean mice by using an in vitro BMP reporter cell assay system, which suggested the presence of

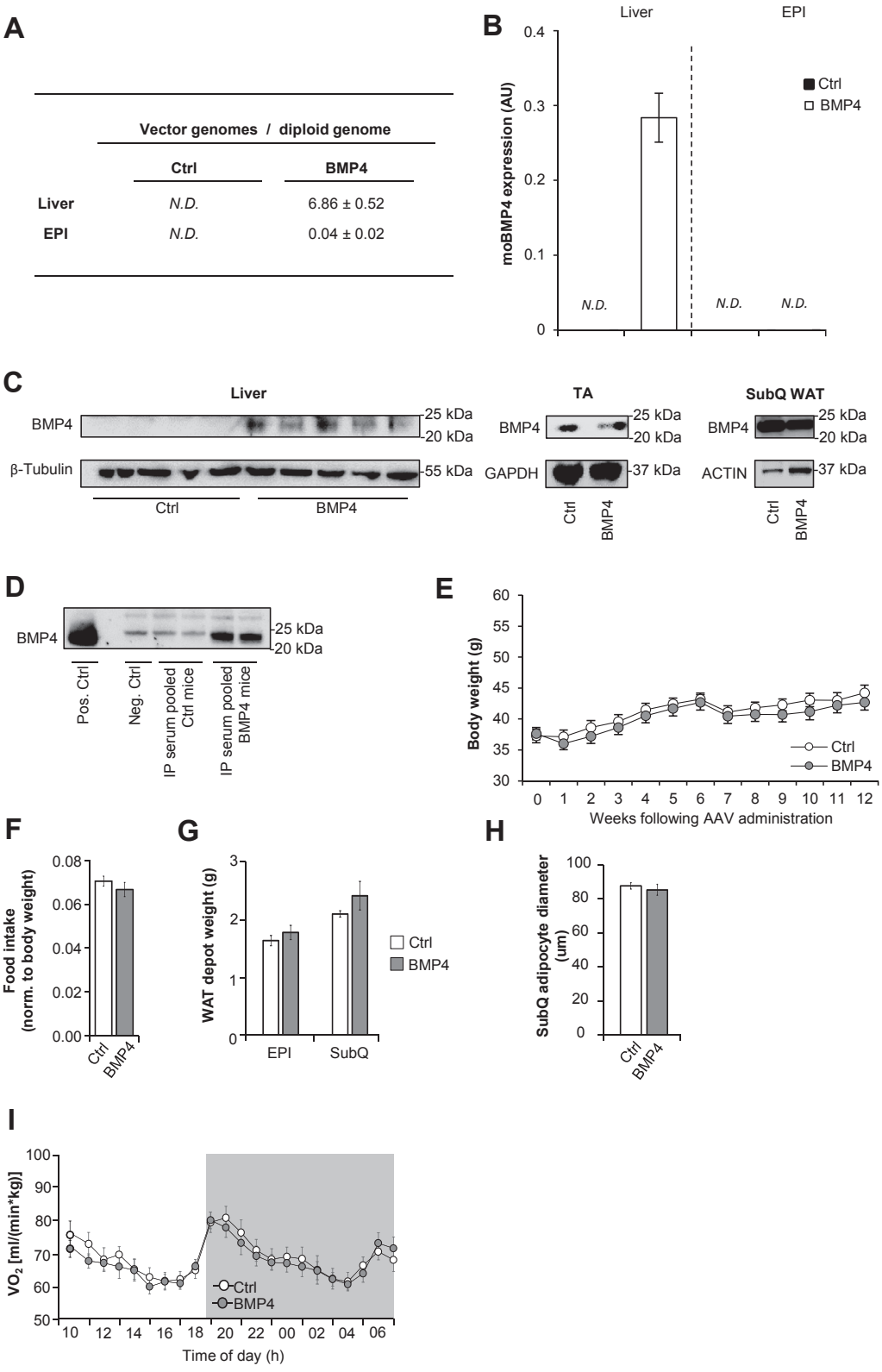

Figure 1: The effect of BMP4 gene therapy on body weight gain in obese mice. Vector gene copy number was determined in DNA isolated from liver and Epi WAT by qPCR with primers specific for BMP4. Liver showed high transduction compared with Epi WAT (**A**). Mouse codon-optimized BMP4 (moBMP4) (described in the Supplemental Methods section) expression was analyzed by RT-qPCR in liver and Epi WAT. *ND*, nondetectable; AU, arbitrary units; Epi WAT, epididymal WAT (**B**). At termination, the AAV8 BMP4 mice had increased BMP4 protein in liver lysates but not in lysates from tibialis anterior (TA) skeletal muscle or subcutaneous (SubQ) WAT (**C**). AAV8 BMP4 mice also had increased circulating BMP4 levels (**D**). Beads and antibody were used as negative control in (**D**). There was no difference in weight gain (**E**) or food intake (**F**) between the groups or in weight of WAT depots (**G**), SubQ adipocyte size (**H**), or oxygen consumption (**I**) between the AAV8 BMP4 mice and control group. All graphs display the means ± SEM. **A-I:** Material from cohort 1. **A-B:** n = 3 + 3. **E-H:** Ctrl n = 15, BMP4 n = 14. (**I**)**:** Ctrl n = 11, BMP4 n = 12. Statistics were calculated using Student's *t*-test.

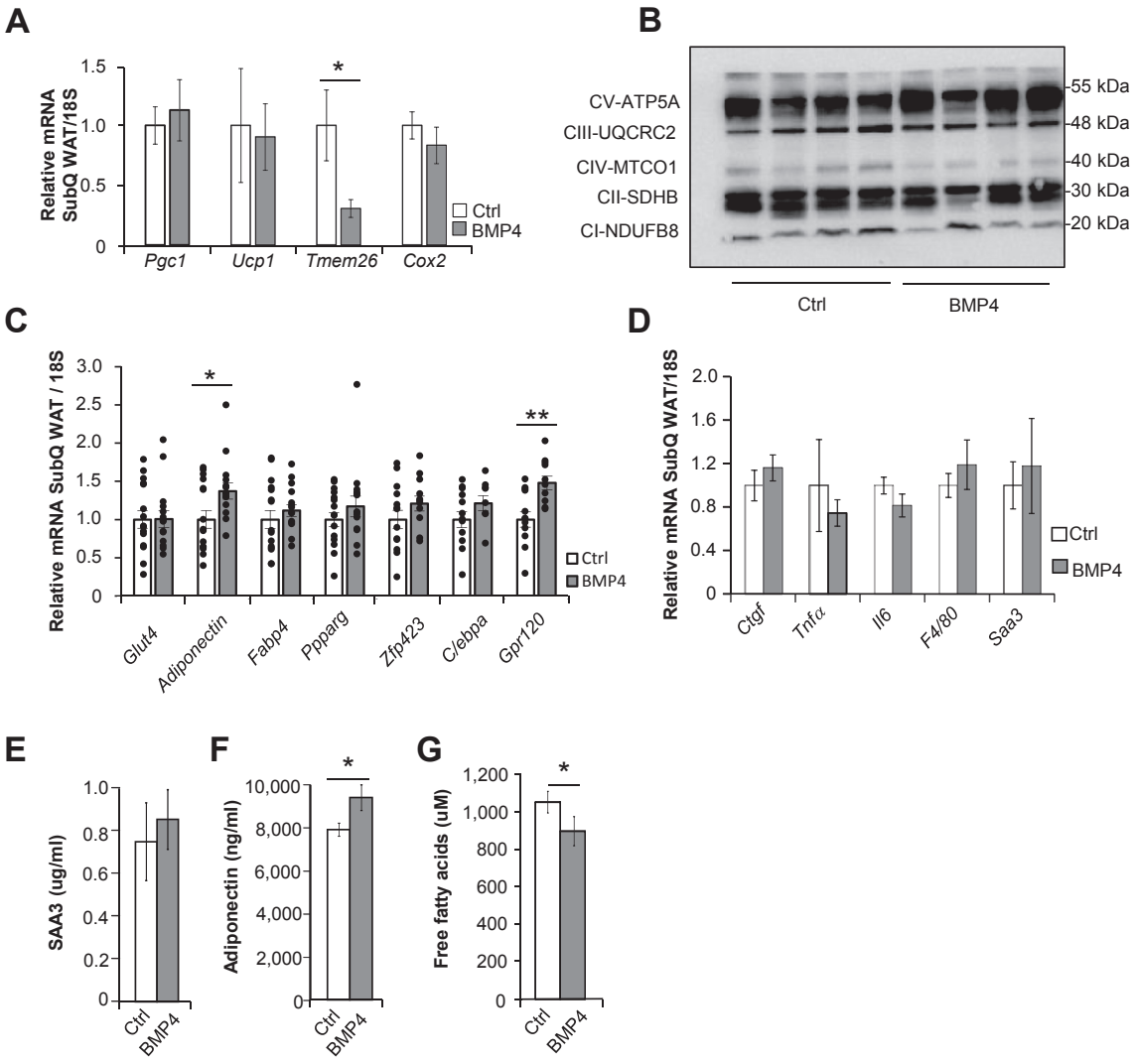

Figure 2: BMP4 gene therapy does not enhance browning of subcutaneous (SubQ) WAT in obesity. There was no increased expression of beige/brown adipocyte genes in subcutaneous (SubQ) WAT in BMP4 mice (**A**) or SubQ WAT mitochondrial OXPHOS proteins (**B**) compared with the control group. Increased markers of adipose cell differentiation in AAV8 BMP4 SubQ WAT but only adiponectin and Gpr120 mRNA levels were significantly increased (**C**). There was no difference in expression of inflammatory and fibrotic genes in SubQ WAT (**D**) and no difference in circulating SAA3 (**E**). AAV8 BMP4 mice had increased levels of circulating adiponectin (**F**) and reduced free fatty acids (**G**) in fasting serum samples. **A-G** show material from cohort 1. Graphs display means ± SEM. **A**: PGC1a, TMEM26, COX2 Ctrl n = 15, BMP4 n = 14. UCP1 Ctrl n = 14, BMP4 n = 12. **B**: n = 4. **C**: GLUT4, adiponectin, FABP4, PPARg Ctrl n = 15, BMP4 n = 14. ZFP423 Ctrl n = 13, BMP4 n = 11. C/EBPa Ctrl n = 12, BMP4 n = 8. GPR120 Ctrl n = 12, BMP4 n = 10. **D**: CTGF, IL6, F4/80, SAA3 Ctrl n = 15, BMP4 n = 14. TNFα Ctrl n = 14, BMP4 n = 13. **E**: Ctrl n = 12, BMP4 n = 11. **F**: n = 14. **G**: Ctrl n = 13, BMP4 n = 14. Statistics in (**G**) were calculated using the Mann—Whitney nonparametric U-test. Statistics were otherwise calculated using Student's *t*-test.

increased circulating BMP antagonists in obesity (Figure 3G). Taken together, increased Noggin and reduced pSMAD 1/5/8 specifically in WAT suggest that the reason for the lack of response to BMP4 therapy in obesity, measured as browning of WAT and body weight reduction, is due to BMP4 resistance in the adipose tissue.

2.4. Improved insulin sensitivity and glucose homeostasis in obese AAV8 BMP4 mice

We next assessed the potential effects of AAV8 BMP4 gene therapy on glucose homeostasis. Ten weeks after AAV8 injections and on continued HFD, the control mice in cohort 1 tended to have further increased fasting insulin levels, while the AAV8 BMP4 mice had significantly lower fasting insulin levels compared with both samples taken prior to (at lower body weights) as well as samples taken 10 weeks after vector administration (Figure 4A). To assess whether this was associated with altered glucose tolerance and insulin sensitivity, the mice underwent an intraperitoneal (i.p.) glucose tolerance test (GTT) and insulin tolerance test (ITT) 10—11 weeks after vector administration. The AAV8 BMP4 mice had significantly better glucose tolerance compared with controls (Figure 4B), with lower insulin levels at baseline after 4 h of fasting and later during the GTT (Figure 4C). Consistent with this, the AAV8 BMP4 mice also had significantly better whole-body insulin sensitivity (Figure 4D, left) and glucose area under the curve (Figure 4D, right). We also performed immunostaining and quantification of pancreatic islet size, which showed no difference between the AAV8 BMP4 and AAV8 control mice (Figure 4E and quantified diagram right). Taken together, these data show that BMP4 enhances insulin sensitivity and that the lower insulin levels during the GTT are a consequence of the improved insulin sensitivity and independent of any effects on body weight.

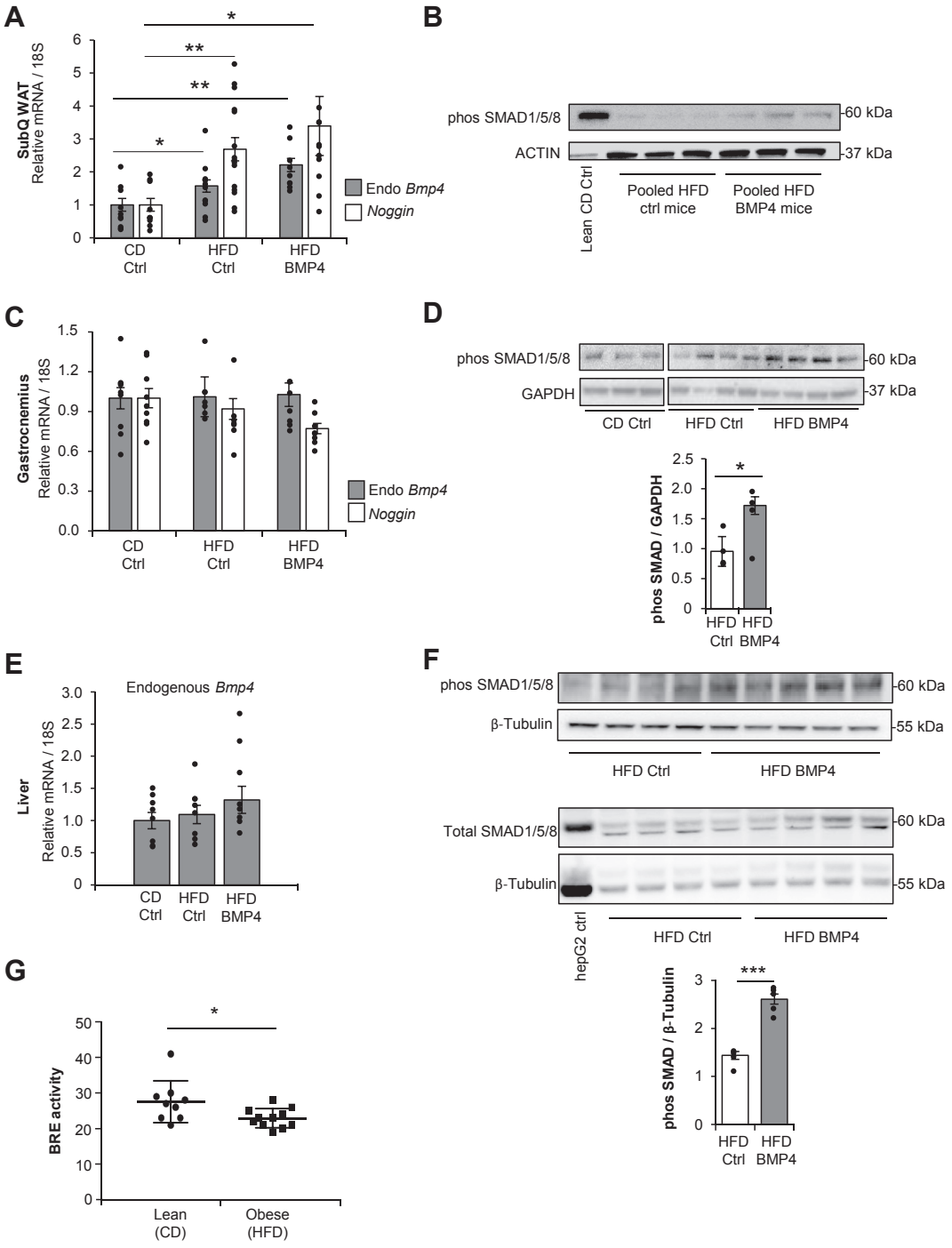

Figure 3: Reduced BMP signaling in subcutaneous adipose tissue but not in skeletal muscle or in liver. Increased mRNA levels of endogenous Bmp4 and the BMP antagonist Noggin in subcutaneous (SubQ) WAT in HFD-fed compared with lean (CD Ctrl) mice (**A**). Low pSMAD1/5/8 activation in lysates of SubQ adipocytes in both obese groups (**B**); BMP4-stimulated lean WT adipocytes were used as positive control in (**B**). Gene expression of endogenous BMP4 and of the antagonist Noggin in gastrocnemius biopsies from lean control mice, compared with obese control and BMP4 mice (**C**). pSMAD1/5/8 is significantly increased in gastrocnemius skeletal muscle from BMP4 obese compared with control obese mice (**D**) (all samples were run on a single, large gel). Gene expression of endogenous BMP4 in liver tissue from lean control and obese AAV8 BMP4 and control mice (**E**). pSMAD1/5/8 is significantly increased in liver tissue in obese AAV8 BMP4 compared with obese control mice; however, the expression of total SMAD 1/5/8 is unchanged (**F**). Reduced BMP-response element activity in C2C12-BRE cells treated with serum from obese (HFD-fed) mice compared with serum from lean (CD-fed) mice (**G**). **A-G** show material from cohort 1. Graphs display means ± SEM. **A**: endo BMP4, Noggin CD Ctrl n = 10, HFD Ctrl n = 13, HFD BMP4 n = 8. **C**: Endo BMP4/Noggin CD Ctrl n = 9, HFD Ctrl/BMP4 n = 8. **E**: CD Ctrl n = 8, HFD/BMP4 n = 8. **G**: lean n = 9, obese n = 11. Statistics were calculated using Student's *t*-test.

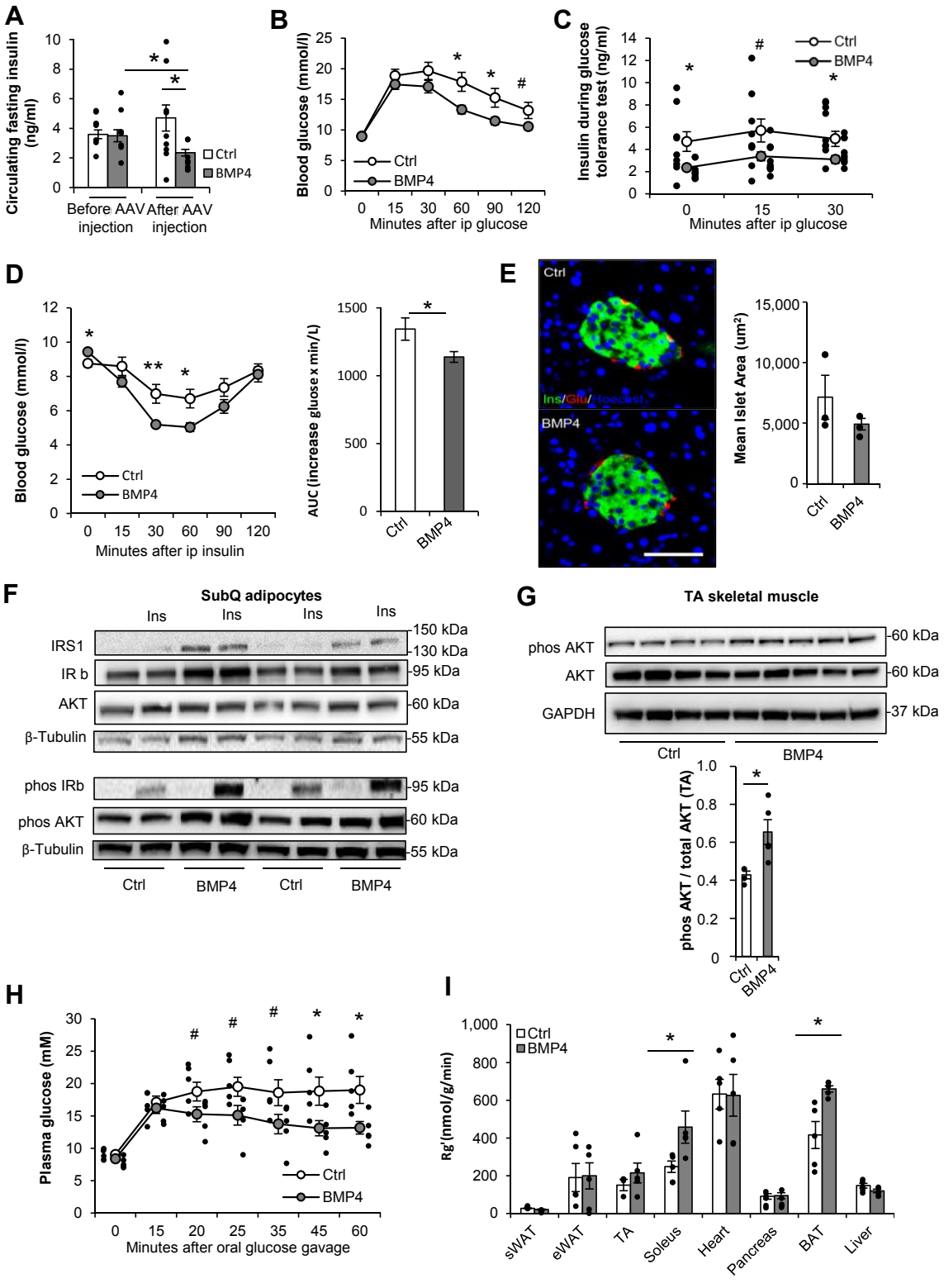

Figure 4: BMP4-treated obese mice have improved insulin sensitivity. Serum insulin levels were similar in both groups before AAV8 injections (**A**). Ten weeks following AAV8 administration and on continued HFD, control mice showed increased insulin levels, while levels were decreased in AAV8 BMP4 mice (**A**). AAV8 BMP4 mice had enhanced glucose tolerance (**B**), lower insulin levels at baseline and during the glucose tolerance test (**C**), and improved insulin sensitivity (**D**). There was no difference in pancreas islet size between the groups (**E**). AAV8 BMP4 mice had significantly increased Insulin Receptor Substrate (IRS) 1 protein and a trend for increased IRb protein in isolated SubQ adipocytes. Insulin-stimulated IRb and AKT phosphorylation were increased in SubQ adipocytes from AAV8 BMP4 compared with control cells, and basal AKT phosphorylation was also increased (**F**). Increased basal AKT phosphorylation in biopsies of tibialis anterior (TA) skeletal muscle from AAV8 BMP4 mice compared with control mice (**G**). Blood glucose levels were decreased during oral administration of glucose (**H**), and the AAV8 BMP4 mice showed tissue-specific increased glucose uptake in soleus skeletal muscle and BAT (**I**). **A-G** show material from cohort 1. **H-I** show material from cohort 2. All graphs show means ± SEM. **A-D**: n = 9, **E**: n = 3, **H-I**: n = 5. Statistics were calculated using Student's *t*-test.

Next, we examined insulin signaling in two target tissues, isolated SubQ adipocytes and skeletal muscle, from the equally obese AAV8 BMP4-treated and -untreated mice. As shown in Figure 4F, insulin receptor substrate 1 (IRS1) protein was increased in BMP4 mice, and IR-b also tended to be increased, whereas there was no difference in AKT protein. Furthermore, insulin-stimulated IR-b phosphorylation (Tyr1146) and downstream pS 473AKT phosphorylation were significantly increased (Figure 4F). We also found significantly increased AKT phosphorylation in excised TA skeletal muscles (Figure 4G and graph below), supporting enhanced insulin sensitivity in skeletal muscles, which is likely an important reason for the increased whole-body insulin effect (Figure 4D).

2.5. Tissue glucose uptake

We then characterized the phenotype of the improved glucose homeostasis in cohort 2 mice, which were treated identically to the mice in cohort 1. We confirmed their similar body weights during the study (Fig. S2c) and the enhanced insulin sensitivity through an ITT (Fig. S2d). To further characterize these mice, we administered oral glucose via gavage and injected ^{14}C-2deoxy-glucose to conscious AAV8 BMP4 and control mice. Similar to cohort 1, BMP4-treated mice from cohort 2 had reduced fasting plasma insulin at baseline (Fig. S2e) and markedly improved whole-body glycemic control following oral glucose (Figure 4H), despite similarly reduced insulin levels as seen in cohort 1 throughout the experiment, thus confirming the increased insulin sensitivity. Tissue-specific glucose uptake (Rg') was significantly increased in the skeletal muscle and BAT of AAV8 BMP4 mice (Figure 4I).

Taken together, these findings in obese mice are consistent with our previous results in lean, AAV8 BMP4-treated mice on a chow diet [5] and show that AAV8 BMP4 has a robust, positive effect on glucose tolerance and insulin sensitivity in both lean and obese mice. Tissue glucose uptake following oral glucose was increased in BAT and skeletal muscle, consistent with the enhanced insulin signaling in skeletal muscle and also seen in white adipocytes.

2.6. BMP4 also enhances hepatic insulin signaling and reduces hepatic gluconeogenic enzymes

We next examined whether BMP4 also could regulate hepatic glucose production. Similar to our findings in WAT, we found markers of increased insulin sensitivity also in the liver in the BMP4 mice from cohort 1 with increased IRb- and IRS1 protein (Fig. S3a blots and quantifications).

To test this in vivo, we performed a pyruvate tolerance test (PTT) to evaluate hepatic gluconeogenesis, which showed a significantly reduced hepatic glucose production in the AAV8 BMP4 mice (Figure 5A). Both fed glucose and insulin levels were significantly decreased in AAV8 BMP4 mice compared with those in controls (Figs. S2f and g), supporting that BMP4 also has positive effects on both hepatic insulin resistance and hepatic gluconeogenesis.

To further validate this, we injected mice in cohort 2 with insulin in the vena cava 5 min prior to sacrifice and evaluated effects on insulin signaling in the liver. Both pS473AKT and pYIRb were increased compared with control mice, showing positive effects of AAV8 BMP4 also on hepatic insulin sensitivity (Figure 5B).

As insulin exerts inhibitory effects on hepatic gluconeogenesis, we asked whether AAV8 BMP4 also suppresses key markers of gluconeogenesis. As shown in Figure 5C, gene expression of key rate-limiting enzymes of gluconeogenesis including glucose 6-phosphatase (*G6pc*), phosphoenolpyruvate carboxykinase 1 (*Pck1*), fructose-1, 6-bisphosphatase 1 (*Fbp1*), and glucokinase (*Gck*) were significantly reduced in the livers of the AAV8 BMP4 mice compared with the equally obese control mice. This effect was not seen in the kidney, which is another gluconeogenic tissue, of the AAV8 BMP4-treated mice (Figure 5D) [11]. Moreover, endogenous BMP4 expression was similar (Figure 5D).

To elucidate whether the effect of BMP4 on gluconeogenesis is mediated by direct suppressive effects on key markers of gluconeogenesis or by enhancing insulin action as in adipose tissue and skeletal muscles, we treated human liver cells (IHH) with recombinant BMP4 alone or with insulin. Interestingly, recombinant BMP4 alone was sufficient to suppress these key markers of gluconeogenesis (Figure 5E). However, BMP4 also enhanced the insulin-induced suppression of the gluconeogenic enzymes (Figure 5E). As expected, Gremlin1, which is a key BMP4 antagonist in human cells, prevented BMP4-induced suppression of the gluconeogenic enzymes and prevented the positive effect of BMP4 with insulin (Figure 5E).

The important role of PGC1-a in the regulation of hepatic gluconeogenesis is well established. Acetylation of PGC1-a has been shown to modulate its activity in several contexts, including gluconeogenesis [12]. We also found that acetylation of hepatic PGC1-a in AAV8 BMP4 mice was significantly increased compared with that of the control mice (Figure 5F).

Collectively, our results show that BMP4 exerts insulin-like effects on the suppression of hepatic gluconeogenic enzymes in both murine and human cells and that this effect could be exerted through modulation of PGC1-a acetylation. The suppressive effect of BMP4 on hepatic gluconeogenesis is also consistent with the markedly improved PTT seen in AAV8 BMP4 mice.

3. DISCUSSION

The current study was designed to determine whether BMP4 gene therapy, shown to prevent the development of obesity [8], could also be a potential treatment for established obesity. However, in contrast to lean mice, BMP4 gene therapy did not reduce body weight or fat mass. Consistent with this, there was no browning of WAT or reduced inflammation or fibrosis, as previously seen in lean mice [5]. This lack of response in WAT was also associated with increased Noggin mRNA and reduced pSMAD1/5/8, supporting that the adipose tissues become BMP4 resistant in obesity in contrast to skeletal muscles and liver. The BMP reporter system data also supported the concept that obesity is a condition of increased BMP antagonism in the circulation, and this may emanate from the expanded adipose tissue. The AAV8-mediated increase in circulating levels of BMP4 were similar to the levels we reported in initially lean AAV8 BMP4 mice [8] but still could not overcome the WAT BMP4 resistance in established obesity. An interesting alternative approach of overcoming adipose tissue BMP4 resistance would thus be to inhibit Noggin in vivo in adult obese mice, and such studies are in development.

We also show for the first time that obese AAV8 BMP4 mice exhibited clear improvement in insulin sensitivity in all key metabolic targets for insulin and also in glucose homoeostasis compared with control mice, despite similar body weight and fat mass. We also found improved whole-body insulin sensitivity in our previous study in lean mice [5], but this could have been secondary to the increased browning of WAT. However, the current study clearly shows that this is not the case. Peripheral tissue glucose uptake following an oral glucose gavage with tracer also showed that the skeletal muscles and BAT had significantly increased glucose uptake, which likely contributes to the improved insulin sensitivity. BAT is a metabolically important tissue in mice for both glucose and lipid metabolism [13]. The increase in insulin-

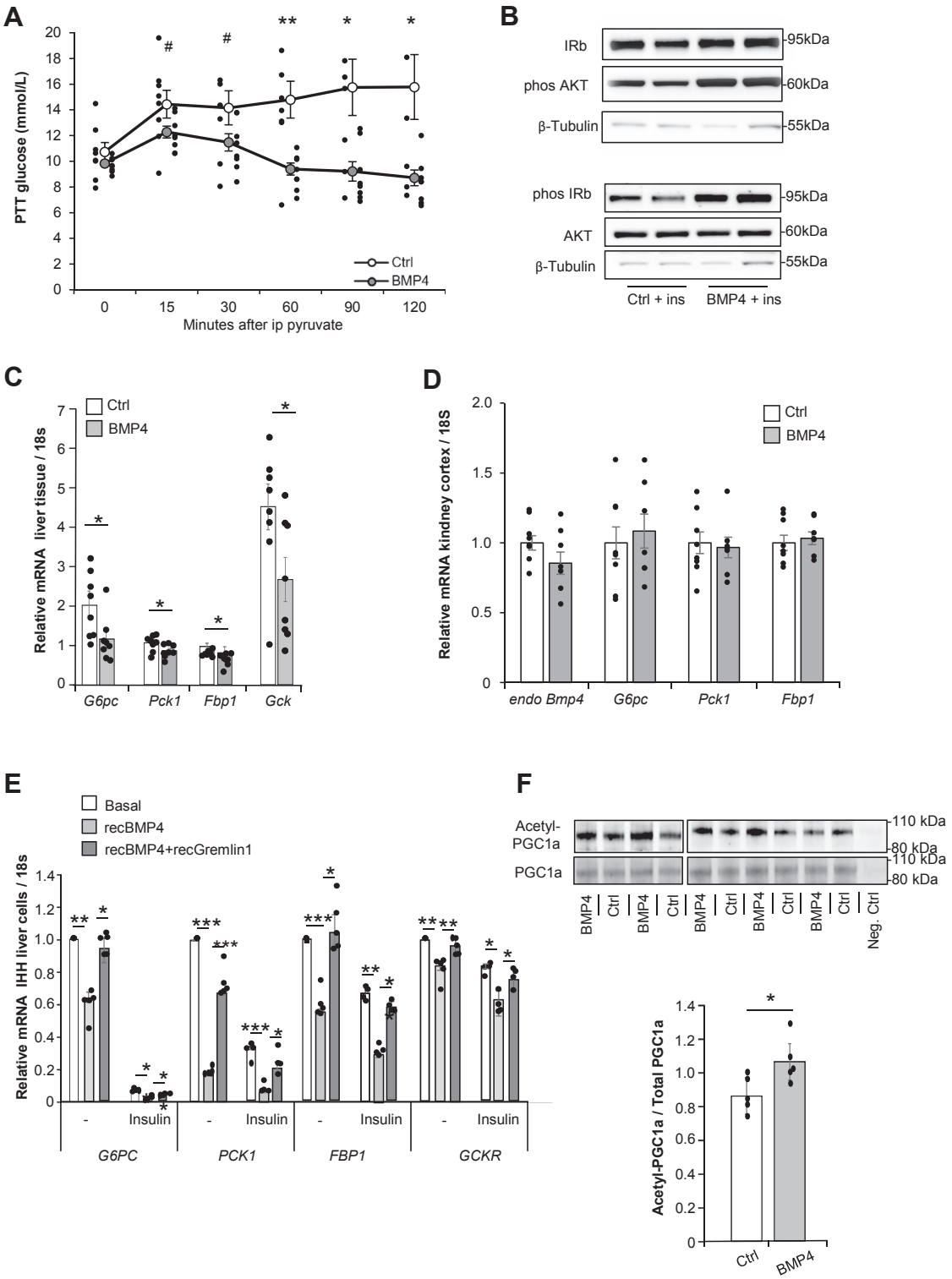

Figure 5: BMP4 treatment reduces hepatic gluconeogenesis and increases PGC1-a acetylation in liver. AAV8 BMP4 mice had improved pyruvate tolerance compared with controls (**A**). Insulin-stimulated hepatic AKT and IRb phosphorylation was increased in obese AAV8 BMP4 mice compared with controls (**B**). Reduced expression of gluconeogenic markers in liver tissue from obese AAV8 BMP4 mice compared with controls (**C**). However, these markers were unaltered in the renal cortex from control diet-fed AAV8 BMP4 mice compared with controls, and endogenous BMP4 levels were also not different (**D**). Recombinant BMP4 treatment of IHH cells also reduced the expression of gluconeogenic markers (**E**). This effect was blunted by recombinant Gremlin1. Acetylated PGC1-a was increased in liver tissue from AAV8 BMP4 mice compared with controls (**F**). Beads and antibody were used as negative control in (**F**). **A** and **B** show material from cohort 2. **C, D,** and **F** show material from cohort 1. All graphs show means ± SEM. **A**: n = 5, **B**: n = 2, **C**: n = 8, **D**: n = 7 + 8, **E**: n = 4–5 (n = 5 for all conditions not stimulated with insulin and n = 4 for all insulin-stimulated conditions), **F**: n = 5. Statistics were calculated using Student's *t*-test.

stimulated glucose uptake in BAT indicates that insulin sensitivity is also increased.

Further detailed studies also showed that all metabolic target tissues for insulin, including WAT, had improved cellular insulin signaling, clearly suggesting that the canonical pSMAD1/5/8 is not a mediator of this effect of BMP4, in contrast to that of browning of the white adipose cells. An additional positive effect of BMP4 was the reduced expression of key hepatic gluconeogenic enzymes in AAV8 BMP4 mice, which may, at least partly, be accounted for by the enhanced hepatic insulin effect. However, a similar direct effect of BMP4 was seen in human liver cells in vitro, and this was additive to that of insulin. Thus, BMP4 exerts direct insulin-like effects in the liver and also enhances the effect of insulin. We could confirm that this is a direct effect of BMP4 since it was antagonized by Gremlin1. Taken together, our results raise the intriguing question of whether BMP4 gene therapy targeting the liver can be used to treat hyperglycemia in animal models of diabetes regardless of obesity. This potential therapeutic approach is currently under investigation.

Our finding of increased PGC1-a acetylation in liver in BMP4-treated mice is also interesting as PGC1-a is a well-known regulator of both hepatic gluconeogenesis and lipid metabolism [12]. Recently, selective inhibition of PGC1-a, by increasing its acetylation, was shown to reduce hepatic gluconeogenesis and improve insulin sensitivity in T2D mice without increasing liver triglycerides or cholesterol levels [14]. In our study, there were also no differences in liver lipid accumulation between AAV8 BMP4 and control mice, as examined by histological staining and triglyceride quantification (Figs. S3b and c). The lower insulin levels as a consequence of the improved insulin sensitivity may also contribute to this. It is well known that chronic hyperinsulinemia in obesity is closely associated with increased hepatic de novo lipogenesis and the associated progression of nonalcoholic fatty liver disease [15]. The detailed molecular mechanisms by which BMP4 gene therapy improves insulin sensitivity in all key metabolic tissues need to be further explored. However, it should also be emphasized that the observed elevated serum adiponectin levels and enhanced transcriptional activation of *Gpr120* in WAT may also contribute to the increased whole-body insulin sensitivity. Both adiponectin and GPR120 activation have previously been shown to improve whole-body insulin sensitivity and enhance cellular insulin signaling [16,17].

4. CONCLUSIONS

Our results show that obesity is a state of BMP4 resistance in WAT, a likely consequence of increased Noggin, but this is not seen in skeletal muscles or in liver. This resistance of local tissue to BMP4 inhibits the positive effects of increased BMP4 on SubQ WAT browning and whole-body energy expenditure, which is seen in lean animals [8]. However, BMP4 still has impressive positive effects on whole-body insulin sensitivity in obese mice with increased insulin signaling in WAT, skeletal muscles, and liver; increased glucose uptake in skeletal muscles and BAT; and also suppressive effects on key markers of hepatic gluconeogenesis. Thus, BMP4 and its antagonists are potential targets in obesity, insulin resistance, and type 2 diabetes.

5. METHODS

5.1. Animals

Male C57BL6/N mice (Taconic, Hudson, NY, USA) were group caged, maintained on a 12-h light–dark cycle in a temperature- (+21 °C) and humidity-controlled room, and underwent weekly weighing. Food and drinking water were administered ad libitum, and the mice were fed an HFD (45 kcal% fat; D12451, Research Diets, New Brunswick, NJ, USA). A first cohort of mice was initially thoroughly characterized; these mice are referred to as cohort 1 throughout the manuscript. Later on, we added a second cohort of mice, referred to as cohort 2, to shed more light on findings from cohort 1. The mice were started on an HFD at 6 weeks of age and kept on the diet until vector administration (study week 0). Upon vector administration, the mice in cohort 1 and 2 were 17 and 18 weeks of age, respectively. The mice were kept on an HFD until the endpoint (12 and 10 weeks after vector administration). For cohort 1, results from the initial GTT and body weights at study week −1 (Figs. S1a and b) were used to match the two groups for subsequent vector administration (described below) at study week 0. Food intake was measured over 1 week. For cohort 2, body weight and fed glucose measurements at study week −1 (Figs. S2a and f) were used to match the two groups for subsequent vector administration at study week 0. At the endpoint, the mice were euthanized using isoflurane (Baxter Medical AB, Kista, Sweden), and blood and tissues were treated as described below for subsequent analyses. Figs. S1c and S2b show the study designs for cohorts 1 and 2. Exact information on which assay was performed in which cohort of mice can be found in the figure legends. All animal experiments were approved by the Research Animal Ethics Committee at the University of Gothenburg, Sweden.

5.2. Recombinant adeno-associated viral vectors

Briefly, recombinant AAV8 encoding a codon-optimized murine Bmp4 cDNA sequence under control of the hAAT promoter was produced by triple transfection of HEK293 cells followed by an optimized cesium chloride gradient-based purification that renders vector batches of high purity [18]. A noncoding plasmid carrying the hAAT promoter was used to produce empty vectors for control mice [19]. The vectors (5×10^{11} viral particles/200 μL saline/mouse; 9 mg/mL saline; Fresenius Kabi, Bad Homburg, Germany) were administered via intravenous tail-vein injection at study week 0 (when the mice were 17 weeks old) [8]. More details of the vectors and biodistribution can be found in the Supplemental methods section.

5.3. GTT, ITT, and PTT

After 4 h of fasting, the mice received i.p. injections containing glucose (1 g/kg body weight [b.w.], Fresenius Kabi), insulin (human recombinant insulin, Actrapid Penfill, Novo Nordisk, Bagsvaerd, Denmark), or pyruvate (2.0 g/kg b.w. pyruvate, Sigma–Aldrich, St. Louis, MO, USA) dissolved in NaCl. Following pilot experiments, the appropriate insulin concentrations were determined to 1.0 U/kg b.w. for cohort 1 and 1.2 U/kg b.w. for cohort 2. Blood samples were collected from the tail vein at 0, 15, 30, 60, 90, and 120 min after injections for subsequent serum analyses. Blood glucose concentrations were determined at these time points using an Accu-Check glucometer (Roche Diagnostics, Basel, Switzerland). Saline (9 mg/mL), insulin (1.0 U/kg b.w.), or glucose solution (1 g/kg b.w.) was given as fluid replacement or to compensate for high or low blood glucose levels.

5.4. Oxygen consumption and activity

Oxygen (VO_2) consumption, carbon dioxide production, and activity were recorded as previously described [8,20] by indirect calorimetry in an INCA Metabolic system (Somedic, Hörby, Sweden) and by use of telemetry devices (MiniMitter, Bend, OR, USA). The measurements were performed 8–9 weeks after vector administration. Data were recorded for 22 h at 20 °C during the light and dark phase. Animals had ad libitum access to food and water. VO_2 was normalized to body weights. Data for the first hour were discarded to account for animal acclimatization.

5.5. Glucose uptake

5.5.1. In vivo protocol

Animals were fasted for 3 h and orally gavaged with glucose (1 g/kg). Fifteen minutes after oral glucose load, ~2.5 μCi of 2-deoxy-D-[^{14}C]-glucose (^{14}C-2DG, Perkin Elmer, Sweden) was administered via i.p. injection ($t = 0$). Blood samples (~20 μL) were collected from the tip of the tail at −16, −1, 5, 10, 20, 30, and 45 min, with plasma glucose measured directly at each time point (Accu-Chek, Roche Diagnostics). Blood samples were immediately centrifuged and stored at −80 °C pending analysis of plasma insulin (Crystal Chem, catalog #90080) and plasma ^{14}C-2DG activity. After 45 min, animals were killed by cervical dislocation and tissues were collected, weighed, placed in a 2-mL tube (Sarstedt, catalog #72.694.007) containing 6 ceramic beads (Retsch, catalog # 5.368.0090), and snap frozen in liquid N_2.

5.5.2. Measurement of plasma and tissue ^{14}C-2DG activity

A 5-μL plasma aliquot was added to 10 mL of scintillation fluid (Optiphase HiSafe 3, PerkinElmer, Sweden, catalog #1200.437) for determination of plasma concentration time course of ^{14}C-2DG. Tissue levels of phosphorylated ^{14}C-2DG (^{14}C-2DG-6-P) were determined following H_2O extraction. Ice-cold Milli-Q H_2O (1.0 mL) was added to each tube, homogenized for 2 × 20 s at 5000 rpm (Precellys 24, Bertin, France) and an additional 5 min at 25 Hz (Mixer Mill 301, Retsch, Germany), and centrifuged (10 min, 10,000 *g* at 4 °C). A 350-μL aliquot of the supernatant was added to 10 mL of scintillation fluid for determination of total tissue ^{14}C-2DG activity (^{14}C-2DG-6-P + ^{14}C-2DG). To isolate ^{14}C-2DG-6-P activity, an additional 350 μL aliquot of the supernatant was loaded on to a solid-phase extraction (SPE) column (Isolute 200 mg PE-AX, Biotage, catalog #503-0020-B). Prior to placing the supernatant on the columns, each SPE column was activated (2 mL, methanol) and equilibrated (2 mL, Milli-Q H_2O). SPE columns were washed with 2 mL Milli-Q H_2O (flow through discarded), and phosphates were eluted, collect with 2 mL 5% NaCl (aq), and added to 10 mL of scintillation fluid. Plasma and tissue ^{14}C activities were measured using liquid scintillation spectrometry (LS6500, Beckman Coulter USA).

5.5.3. Calculation of tissue-specific glucose clearance (K_g') and utilization (R_g') indices

The clearance rate of ^{14}C-2DG-6-P (K_g'), represents an index of the ability of a particular tissue to USE (metabolize) glucose, calculated using the relation:

$$K'_g = \frac{m_{DG-6-P}}{\int_0^T c_{DG}(t)dt}$$

where $m_{DG\text{-}6\text{-}P}$ is the activity of ^{14}C-2DG-6-P per unit tissue mass (dpm/g) at the end of the experiment, $c_{DG}(t)$ is the plasma concentration time course of ^{14}C-2DG and T is the total ^{14}C-2DG exposure time (i.e., experiment length, 45 min). The glucose metabolic index or estimate of glucose utilization (R_g') is calculated from K_g' by the equation:

$$R'_g = C_G \cdot K'_g$$

where C_G is the average plasma glucose concentration during the ^{14}C-2DG exposure time.

5.6. In vivo insulin stimulation

In vivo insulin stimulation was performed as previously described [21]. In brief, animals were fasted for 3 h and anesthetized with an i.p. injection of pentobarbital (120 mg/kg). Insulin was injected (5 mU/g) through the inferior vena cava. After 5 min, tissues were harvested. Tissues were homogenized and lysed at 4 °C, and lysates were subjected to Western blotting to assess insulin-stimulated phosphorylation cascades.

5.7. Serum chemistry

Insulin (Ultrasensitive Mouse Insulin ELISA kit #90080, Chrystal Chem Inc., Downers Grove, IL, USA), adiponectin (Quantikine ELISA, MRP300 R&D Systems, Minneapolis, MN, USA), free fatty acids (kit #ab65341, Abcam, Cambridge, UK), and serum amyloid A isoform 3 (SAA3) (#EZMSAA3-12K, Merck Millipore, Darmstadt, Germany) were measured in serum according to the protocols provided by the manufacturers.

5.8. Liver triglyceride content

Triglyceride content (Kit #10010303, Cayman Chemicals, Ann Arbor, MI, USA) was measured in liver biopsies according to the protocol provided by the manufacturer.

5.9. Insulin stimulation

5.9.1. Isolated adipocytes

Isolation was performed essentially as described [8,22]. Briefly, biopsies of SubQ WAT were washed, cut, and incubated with collagenase (1 mg/mL; Sigma−Aldrich). The isolated adipocytes were filtered through a 250-μm nylon mesh and washed. Adipocyte diameter was measured as previously described [5,22]. Adipocytes were stimulated with 1 nM human recombinant insulin (Actrapid Penfill) for 15 min.

5.9.2. Human hepatocyte cell line (IHH)

Cells were seeded on gelatin-coated plates and cultured in Williams E medium (Life Technologies, MA, USA), supplemented with 10% fetal bovine serum. For insulin signaling analysis, the cells were starved for 16 h with 0.1% serum and incubated with recombinant BMP4 (50 ng/mL), recombinant Gremlin1 (200 ng/mL), and/or insulin (10 nM), followed by protein and RNA extractions.

5.10. Immunoprecipitation

5.10.1. Immunoprecipitation of BMP4

Pooled serum from control and BMP4 mice were precleaned using A/G PLUS-Agarose beads (Santa Cruz Biotechnology, Dallas, TX, USA), immunoprecipitated with a BMP4 antibody (sc-73536, Santa Cruz Biotechnology, Dallas, TX, USA), and analyzed by subsequent immunoblotting. Beads and antibody were used as a negative control. Recombinant BMP4 protein was used as positive control.

5.10.2. Immunoprecipitation and acetylation analysis of PGC1-a

Liver tissue lysates obtained from AAV8 control and AAV8 BMP4 mice were precleaned with A/G PLUS-Agarose beads before immunoprecipitation with a PGC1-a antibody (sc-13067, Santa Cruz Biotechnology, Dallas, TX, USA). Samples were then immunoblotted with same PGC1-a antibody or acetylated-lysine antibody (#9681, Cell Signaling). Beads and antibody were used as a negative control.

5.11. BMP reporter assay

BMP-reporter assay experiments were performed essentially as previously described [23]. Briefly, stably transfected C2CL2-BRE cells, containing the pGL3-luciferase reporter construct fused to BMP-specific response elements (BRE) from the Id1-promoter, were allowed to attach overnight before starvation in DMEM, 0.1% fetal bovine serum (FBS) for 6 h. After starvation, cells were incubated with DMEM, 0.1% FBS supplemented with 2% mouse serum for 20 h, after which luciferase activity was measured. The quantified luciferase signal was related to total protein concentration.

5.12. Immunoblotting

Immunoblotting was performed essentially as described [3], with the following primary antibodies: total OXPHOS Antibody Cocktail (ab110413, Abcam); p IR/IGF beta (3021), p AKT (9271), AKT (9272), p38 MAPK (9212), p p38 MAPK (9211), HSL (4107), p SMAD1/5/8 (13820), and B tubulin (2128) (all from Cell Signaling Technology, Danvers, MA, USA); IRS1 (06–248, Upstate/Merck Millipore); IR beta (sc-711), p JNK (sc-6254), BMP4 (sc-73536), SMAD 1/5/8 (N-18)-R (sc 6031-R), GAPDH (sc-47724), and actin (sc-8432) (all from Santa Cruz Biotechnology, Dallas, TX, USA); and UCP1 (MAB6158, R&D Systems). Recombinant mouse BMP4 (R&D Systems) was used as a positive control where indicated. Quantifications were performed with normalization against loading controls.

5.13. Measurement of islet size

Paraffin-embedded paraformaldehyde-fixed pancreases were sectioned in 200-μm increments and stained with polyclonal guinea pig anti-insulin antibody (1:1000, Dako, Jena, Germany) and mouse monoclonal anti-glucagon antibody (1:2000, Sigma–Aldrich). Secondary antibodies used were Alexa Fluor™ 488 anti-guinea pig and Alexa Fluor™ 594 anti-mouse (Thermo Fisher Scientific, Waltham, MA, USA), essentially as described [24]. Islet size was determined by measuring the insulin and glucagon area of 50 islets per mouse.

5.14. Gene expression analysis

Real-time RT-PCR gene expression analysis was performed as described [8] using the TaqMan System and normalized to 18S RNA. Gene-specific primers and probes were designed using the software Primer Express or purchased on demand (all from Applied Biosystems, Carlsbad, CA, USA). Sequences and assay IDs are available upon request.

5.15. Statistical calculations and figures

Statistics were performed using Excel (Microsoft Office, Redmond, WA, USA) or IBM SPSS Statistics version 24 (IBM, Armonk, NY, USA). Comparisons were performed using two-tailed Student's *t*-test or Mann–Whitney nonparametric U-test (stated in figure legends). Results are reported as means ± SEM. Individual data points are included in figures where $n \leq 10$. Significances are indicated in figures according to the following: $\#p < 0.1$, $*p < 0.05$, $**p < 0.01$, $***p < 0.001$.

AUTHOR CONTRIBUTIONS

U.S., S.H., J.M.H., and A.H. designed the experiments; J.M.H., J.G., A.H., J.B., T.K., and S.M. performed animal husbandry and mouse in vivo experiments; and J.M.H., S.H., and T.G. performed the in vitro work. F.B. and I.E. generated and characterized the viral vectors, and V.P. contributed to the energy expenditure and activity measurements. U.S., S.H., and J.M.H. wrote the final article, and all authors approved and contributed.

FUNDING

This work was funded by the Swedish Research Council, the Swedish Diabetes Association, the Novo Nordisk Foundation, the Torsten Söderberg Foundation, the Edgar Sjölund Foundation, the EFSD/Lilly European Diabetes Research Programme, and the West Sweden ALF program.

ACKNOWLEDGEMENTS

We thank our colleagues at the Lundberg Laboratory for Diabetes Research for fruitful discussions.

CONFLICT OF INTEREST

None declared.

APPENDIX A. SUPPLEMENTARY DATA

Supplementary data to this article can be found online at https://doi.org/10.1016/j.molmet.2019.11.016.

REFERENCES

[1] Wang, Q.A., Tao, C., Gupta, R.K., Scherer, P.E., 2013. Tracking adipogenesis during white adipose tissue development, expansion and regeneration. Nature Medicine 19:1338–1344.

[2] Bowers, R.R., Lane, M.D., 2007. A role for bone morphogenetic protein-4 in adipocyte development. Cell Cycle 6:385–389.

[3] Hammarstedt, A., Hedjazifar, S., Jenndahl, L., Gogg, S., Grünberg, J.R., Gustafson, B., et al., 2013. WISP2 regulates preadipocyte commitment and PPARgamma activation by BMP4. Proceedings of the National Academy of Sciences of the United States of America 110:2563–2568.

[4] Gustafson, B., Hammarstedt, A., Hedjazifar, S., Hoffmann, J.M., Svensson, P.A., Grimsby, J., et al., 2015. BMP4 and BMP antagonists regulate human white and beige adipogenesis. Diabetes 64:1670–1681.

[5] Gustafson, B., Smith, U., 2012. The WNT inhibitor Dickkopf 1 and bone morphogenetic protein 4 rescue adipogenesis in hypertrophic obesity in humans. Diabetes 61:1217–1224.

[6] Wang, G., Zhang, H., Zhao, Y., Li, J., Cai, J., Wang, P., et al., 2005. Noggin and bFGF cooperate to maintain the pluripotency of human embryonic stem cells in the absence of feeder layers. Biochemical and Biophysical Research Communications 330:934–942.

[7] Topol, L.Z., Bardot, B., Zhang, Q., Resau, J., Huillard, E., Marx, M., et al., 2000. Biosynthesis, post-translation modification, and functional characterization of Drm/Gremlin. Journal of Biological Chemistry 275:8785–8793.

[8] Hoffmann, J.M., Grünberg, J.R., Church, C., Elias, I., Palsdottir, V., Jansson, J.O., et al., 2017. BMP4 gene therapy in mature mice reduces BAT activation but protects from obesity by browning subcutaneous adipose tissue. Cell Reports 20:1038–1049.

[9] Qian, S.W., Tang, Y., Li, X., Liu, Y., Zhang, Y.Y., Huang, H.Y., et al., 2013. BMP4-mediated brown fat-like changes in white adipose tissue alter glucose and energy homeostasis. Proceedings of the National Academy of Sciences of the United States of America 110:E798–E807.

[10] Modica, S., Straub, L.G., Balaz, M., Sun, W., Varga, L., Stefanicka, P., et al., 2016. Bmp4 promotes a Brown to white-like adipocyte shift. Cell Reports 16:2243–2258.

[11] Triplitt, C.L., 2012. Understanding the kidneys' role in blood glucose regulation. American Journal of Managed Care 18:S11—S16.
[12] Finck, B.N., Kelly, D.P., 2006. PGC-1 coactivators: inducible regulators of energy metabolism in health and disease. Journal of Clinical Investigation 116: 615—622.
[13] Stanford, K.I., Middelbeek, R.J., Townsend, K.L., An, D., Nygaard, E.B., Hitchcox, K.M., et al., 2013. Brown adipose tissue regulates glucose homeostasis and insulin sensitivity. Journal of Clinical Investigation 123:215—223.
[14] Sharabi, K., Lin, H., Tavares, C.D.J., Dominy, J.E., Camporez, J.P., Perry, R.J., et al., 2017. Selective chemical inhibition of PGC-1α gluconeogenic activity ameliorates type 2 diabetes. Cell 169:148—160.
[15] Tilg, H., Moschen, A.R., Roden, M., 2017. NAFLD and diabetes mellitus. Nature Reviews Gastroenterology & Hepatology 14:32—42.
[16] Awazawa, M., Ueki, K., Inabe, K., Yamauchi, T., Kubota, N., Kaneko, K., et al., 2011. Adiponectin enhances insulin sensitivity by increasing hepatic IRS-2 expression via a macrophage-derived IL-6-dependent pathway. Cell Metabolism 13:401—412.
[17] Oh, D.Y., Walenta, E., Akiyama, T.E., Lagakos, W.S., Lackey, D., Pessentheiner, A.R., et al., 2014. A Gpr120 selective agonist improves insulin resistance and chronic inflammation in obese mice. Nature Medicine 20:942—947.
[18] Ayuso, E., Mingozzi, F., Montane, J., Leon, X., Anguela, X.M., Haurigot, V., et al., 2010. High AAV vector purity results in serotype- and tissue-independent enhancement of transduction efficiency. Gene Therapy 17: 503—510.
[19] Vilà, L., Elias, I., Roca, C., Ribera, A., Ferré, T., Casellas, A., et al., 2014. AAV8-mediated Sirt1 gene transfer to the liver prevents high carbohydrate diet-induced nonalcoholic fatty liver disease. Molecular Therapy Methods and Clinical Development 1.
[20] Wernstedt, I., Edgley, A., Berndtsson, A., Fäldt, J., Bergström, G., Wallenius, V., et al., 2006. Reduced stress- and cold-induced increase in energy expenditure in interleukin-6-deficient mice. American Journal of Physiology — Regulatory, Integrative and Comparative Physiology 291:R551—R557.
[21] Jing, E., Emanuelli, B., Hirschey, M.D., Boucher, J., Lee, K.Y., Lombard, D., et al., 2011. Sirtuin-3 (Sirt3) regulates skeletal muscle metabolism and insulin signaling via altered mitochondrial oxidation and reactive oxygen species production. Proceedings of the National Academy of Sciences of the United States of America 108:14608—14613.
[22] Rotter, V., Nagaev, I., Smith, U., 2003. Interleukin-6 (IL-6) induces insulin resistance in 3T3-L1 adipocytes and is, like IL-8 and tumor necrosis factor-alpha, overexpressed in human fat cells from insulin-resistant subjects. Journal of Biological Chemistry 278:45777—45784.
[23] Herrera, B., Inman, G.J., 2009. A rapid and sensitive bioassay for the simultaneous measurement of multiple bone morphogenetic proteins. Identification and quantification of BMP4, BMP6 and BMP9 in bovine and human serum. BMC Cell Biology 10.
[24] Lof-Ohlin, Z.M., Nyeng, P., Bechard, M.E., Hess, K., Bankaitis, E., Greiner, T.U., et al., 2017. EGFR signalling controls cellular fate and pancreatic organogenesis by regulating apicobasal polarity. Nature Cell Biology 19:1313—1325.

